Applied Microscopy
Korean Society of Microscopy

pISSN 2287-5123 · eISSN 2287-4445
http://dx.doi.org/10.9729/AM.2013.43.1.40

Mn-deprived Phase Transformation in High-Mn Steel during the Dew-point Control Process

Woong-Pyo Hong, Sung-Il Baik, Gyo-Sung Kim[1], Sun-Ho Jeon[1], Kwang-Guen Chin[1], Chang-Seok Oh[2], Young-Woon Kim*

Department of Materials Science and Engineering, Research Institute of Advanced Materials, Seoul National University, Seoul 151-744, Korea,
[1]POSCO Technical Research Laboratory, Gwangyang 545-875, Korea
[2]Korea Institute of Materials Science, Changwon 641-831, Korea

*Correspondence to:
Kim YW,
Tel: +82-2-880-7977
Fax: +82-2-883-8197
E-mail: youngwk@snu.ac.kr

Received March 17, 2013
Revised March 20, 2013
Accepted March 20, 2013

Phase transformation by the Mn-deprivation was observed in the high-Mn twinning-induced plasticity-aided steel. Mn-depletion was induced by the formation of Mn-O oxide during the dew-point control process at temperature above –20°C, which changed austenitic parent phase to multi-grained ferrite. Mixture of Al-O, Al-Mn-Si-O oxides were observed at the grain boundaries of transformed ferrite.

Key Words: Alloys, Surface modification, Phase transformation, Oxidation, Transmission electron microscopy

INTRODUCTION

Since the first introduction of high-Mn steel by Hadfield (Hadfield, 1956), effects of Mn addition were widely studied in the fields of damping, corrosion, toughness, and strengthening (Sato et al., 1982; Tomota et al., 1987; Grässel et al., 2000; Gavriljuk et al., 2006). Because of its excellent strength with high elongation, Fe-Mn-based twinning-induced plasticity (TWIP)-aided steel drew much attention in the recent industry applications for the high-performance components in the automobile. One of the hurdles for TWIP-aided steel to overcome is the surface protection to be used in the automobiles utilizing its excellent mechanical properties. Surface of steel sheets used in the automobiles is usually protected by Zn coating. When zinc is coated in the molten Zn bath, dew-point (DP) controlled process is critically required to reduce the surface oxides or change stoichiometry of oxides to make good adhesion of Zn. Mn-O and Si-O are known as non-wetting oxides with Zn, and should be converted to other types of oxides, or reduced, by proper DP control process to minimize the "bad-spots", i.e., non-wetting spots of Zn. It is generally known that the content of manganese higher than 2 wt% causes Zn adhesion problems forming non-wetting spots. TWIP-aided steel typically contains more than 10 wt% of Mn (Mintz, 2001), which provides a potential source of Mn-O oxides.

In the most of the surface studies with high-Mn content assumes the surface with austenitic phase because Mn is an austenitic phase stabilizer in steel alloying. However, it was found in this study that the formation of Mn-O oxide on the surface resulted in the deprivation of Mn in the sub-surface layer, which turned the austenitic phase to ferrites.

MATERIALS AND METHODS

The composition of the TWIP-aided steels used in this study was 0.6C-18Mn-1.5Al-0.1Si in wt%. Oxidized samples went through DP controlled process at 800°C under gas mixture of N_2 with fractional H_2O balanced to set different DP temperatures from 0 to –60°C. Holding time was fixed for

This research was supported by the Nano-Material Technology Development Program (the Green Nano Technology Development Program) through the National Research Foundation of Korea funded by the Ministry of Education, Science and Technology (2011-0019984).

40 and 60 seconds with the above DP processing. Surface of the surface-treated samples were scanned using Kratos AXIS HSi X-ray photoelectron spectroscopy (XPS) to identify the chemical states of surface oxides. Thermo-Calc (Thermo-Calc, Stockholm, Sweden) was used to map the stable oxides when DP was changed at the treatment temperature of 800°C with the TWIP-aided steel composition used. Cross-sectional ion channeling images were obtained using focused ion beam (FIB). Cross-sectional transmission electron microscopy (XTEM) samples were prepared by mechanically thinning followed by 4 kV argon ion-milling using single modulation technique in Gatan Precision Ion Polishing System (Gatan, Pleasanton, CA, USA). Prior to XTEM sample preparation, gold was coated at the top surface to protect the oxides formed at the outermost surface. Distributions and types of the oxide were investigated using annular dark-field (ADF) imaging, electron diffraction, and energy dispersive spectroscopy (EDS) in JEOL JEM-2010F and FEI F20 transmission electron microscopes, operated at 200 kV. ADF imaging, known as Z-contrast, was mainly adopted because oxides were difficult to discern in normal bright-field image.

RESULTS

Fig. 1 shows the XPS peaks of Mn, Si, Al and O from the samples annealed at different DPs, 0, –20, –40 and –60°C. Oxide distributions showed distinct transition with two groups with the DP ranging –20°C and above, and equal to –40°C or below in XPS analysis. Mn peaks, possibly from MnO_2 and Mn_2O_3, were observed in Mn energy spectrum from all 4 samples as shown Fig. 1A. Si and Al peaks did not appear from the samples processed at –20°C and above, which indirectly indicated that the Al and Si oxides were not formed at the surface, or might be formed below the surface. Splitting and shift of oxygen peaks from 530.6 to 531.5 eV in Fig. 1B, revealed that there was transition of oxides from MnO_2 to $MnSiO_3$ (or Mn_2SiO_4) as DP temperature decreased, which was also known to deteriorate the wettability of Zn. In the samples processed at DP of –40°C and below, Al energy

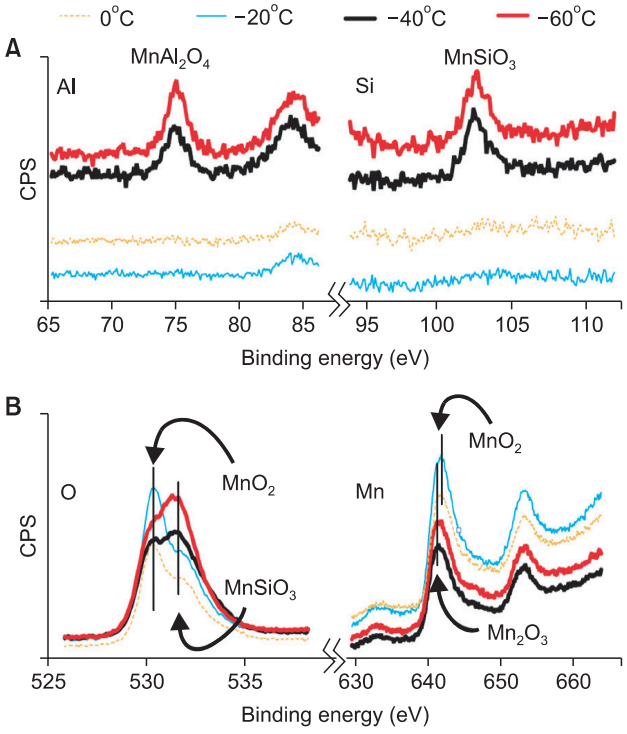

Fig. 1. (A) X-ray photoelectron spectroscopy spectrum of Mn, O, SI and Al from samples processed at 4 different dew-point (DP) temperature, 0, –20, –40, and –60°C. Samples processed at DP temperature of –20°C and above shoed clear difference in the oxide formation compared with the ones processed at –40°C DP and below. (B) Energy spectrum showing the oxygen and manganese bonding nature. It shows the transition of oxygen bonding from MnO_2 bonding to $MnSiO_3$ as lowering DP temperature, which also changes Manganese bonding MnO_2 to Mn_2O_3. CPS, counts per seconds.

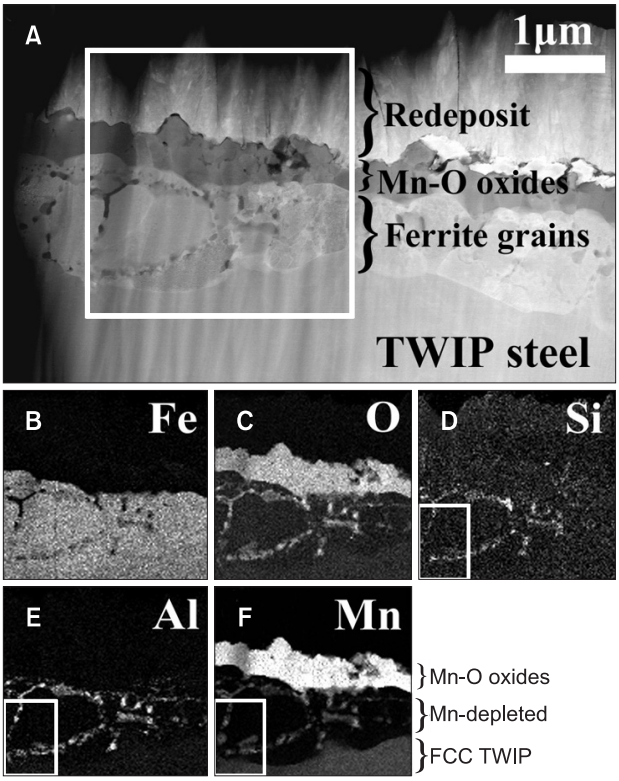

Fig. 2. (A) Annular dark-field image of cross-sectional view of the sample processed at 800°C with dew-point temperature of 0°C. (B-F) Elemental distribution of Fe, Mn, Al, Si, and O in the near-surface region, respectively. Mapped area is marked with a rectangle in (A). Mn-depleted region changed the face centered cubic (FCC) austenite matrix to body centered cubic ferrite. Oxygen penetrated into the matrix through the ferrite grain boundaries to form Al-Si-O oxides. Rectangle area in (D-F) show the difference of element distribution. TWIP, twinning-induced plasticity.

spectrum were fitted with the energy of 74.6 eV, indicating the formation of $MnAl_2O_4$.

Fig. 2A and B show the XTEM ADF image and the elemental distribution, respectively, from the sample annealed with 0°C DP in pure N_2 gas environment. Top-most layer in XTEM of Fig. 2A was from the re-deposits during the single-modulated ion milling process. Two types of oxides were identified - thick surface oxide at the surface and the networked oxides below. Top surface oxide had about 0.5 μm-thick layer and mainly consisted of Mn and O, with no traces of Al and Si. In the Mn distribution of Fig. 2B, it revealed depletion layer of Mn, about 2 μm-deep from the surface, which indicated that Mn diffused out from the matrix to form the top Mn-O oxides.

Region with Mn depletion, the area right below the surface Mn-O oxides, was investigated using conventional transmission electron microscopy from cross-sectional sample, which is shown in Fig. 3. Fig. 3A is a brightfield image of region investigated and Fig. 3B is a selected area electron diffraction patterns including the visible area in Fig. 3A. Diffraction spots from ferrite phase [110] planes, marked with arrows, are visible with no diffraction spots from austenite phase. Electron diffraction patterns of Fig. 3A①-④ were obtained from individual grains marked as rectangles ①-④ in Fig. 3A, respectively. All electron diffraction patterns from individual grains showed single crystal ferrite phase. All electron diffraction patterns of ①-④ were obtained by tilting the sample to get zone axis pattern. Depletion of Mn turned the austenitic matrix into polycrystalline ferrite, which did not have specific crystallographic relationship with matrix as confirmed by electron diffractions from individual grains.

In order to confirm that the phase transformations observed in transmission electron microscopy was the representative results of generic area, ion channeling image from FIB was obtained and compared with the XTEM results. Fig. 4 shows the near-surface structure at low magnification using ion

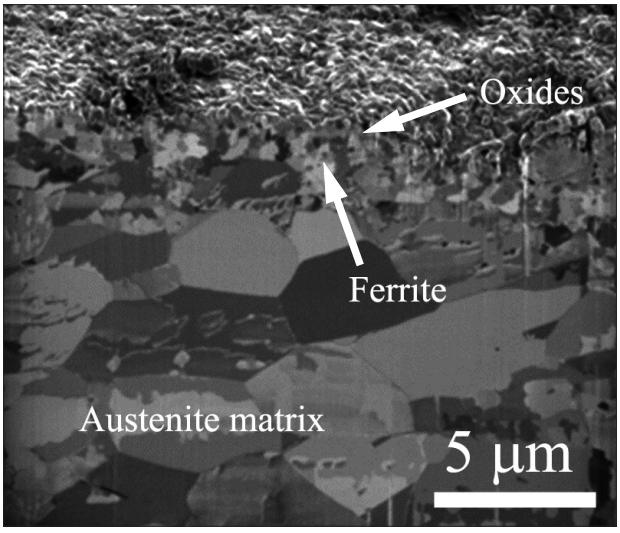

Fig. 4. Ion channeling image from focused ion beam. Cross-sectional view of the near-surface region reveals Mn-O oxide, transformed ferrite, and austenitic twinning-induced plasticity matrix from the surface side.

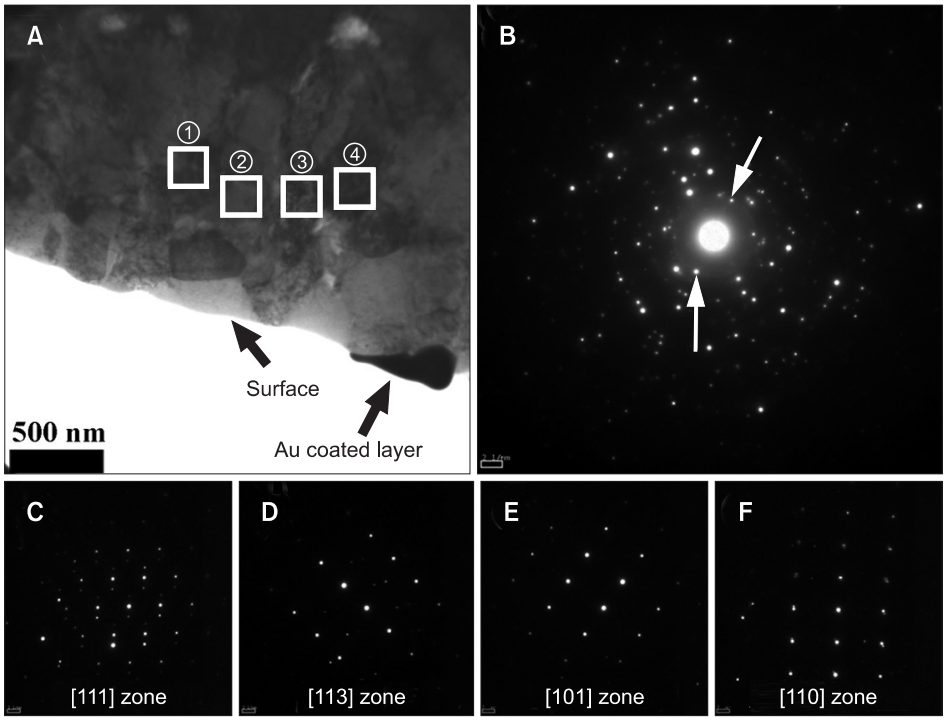

Fig. 3. (A) Brightfield image of area just below the Mn-O oxide showing the transformed ferrite from the matrix. (B) Selcted area diffraction pattern of area (A). Two arrows represent the shortest g-vector of ferrrite [110]. (C-F) show the electron diffraction pattern obtained from area ①-④ marked in (A), respectively.

channeling from FIB. Cross-sectional ion channeling image clearly shows that the band of small grains right below Mn-O oxides with comparable thickness observed in XTEM.

Ferrite grain boundaries were precipitated with Al-O and Al-Si-Mn-O oxides as shown in the elemental distribution of Fig. 2B. Unlike typical internal oxidation, networked oxides were not aligned normal to the surface (Li et al., 2008), which might be due to the short process time giving not enough time for oxygen to diffuse. When the holding time increased to 60 seconds at 800°C with 0°C DP, internal oxides, aligned normal to the surface, were observed. Networked oxides contained complex oxides including Al, Si, Mn, and O. A close investigation revealed that the Al-Si-O oxides appeared in the center of oxides and were surrounded by the Mn-O oxide. Layered structure of Al-Si-O and Mn-O meant that the formation of oxides was governed by the relative diffusivities of elements. It was believed that the ferrite grain boundaries worked as fast diffusion paths for Mn because the calculation of the diffusion length based on the bulk diffusivity of Mn is shorter than the depletion depth (Huin et al., 2005).

Fig. 5 shows the cross-sectional view of the sample processed at –20°C DP with corresponding elemental mapping. Ferrite formation from Mn depletion and the surface Mn-O oxide layer were observed similar to the sample processed at 0°C. The thicknesses of top Mn-O oxide layer and the Mn-depletion layers, however, were reduced to about 300 nm and 700 nm, respectively. By lowering the DP by –20°C, formation of networked oxides was suppressed and the oxides in the ferrite grain boundaries contained only Al and O, with no traces of Si or Mn. There existed thin layer of Al-Si-O oxides in between the top Mn-O oxides and Mn-depleted ferrite grains, which was not observed in the sample processed at 0°C DP.

Fig. 6 shows XTEM image of the microstructure and the distribution of elements in the sample oxidized at DP –40°C, where oxide distributions were completely different from the samples processed at higher DP temperatures. Thick, top Mn-O oxide layer and the depletion layer of Mn were not observed. Oxides containing Mn, Si, and O were buried below the surface, which was about 250 nm-deep from the surface, and the layered structure of Al-O was observed. Some of the AlN precipitates were formed along the austenitic TWIP-aided steel grain boundaries as deep as 500 nm below the

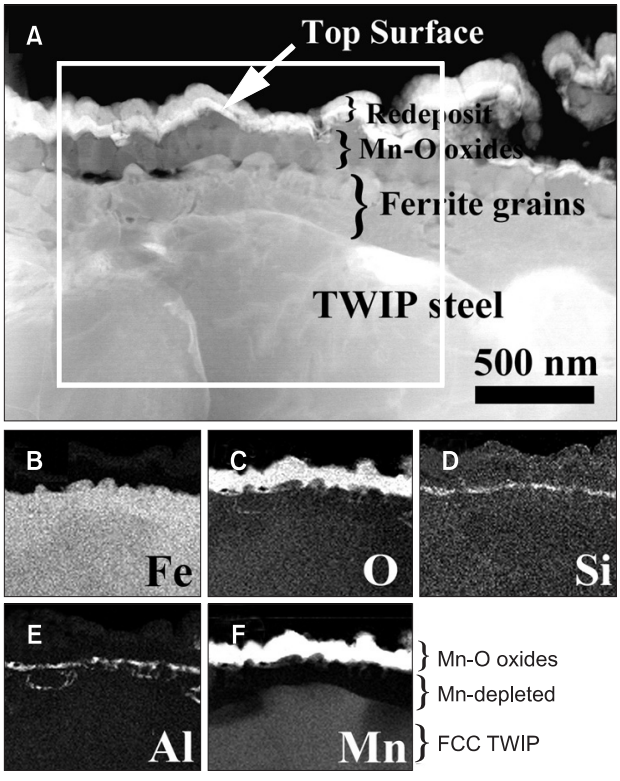

Fig. 5. (A) Annular darkfield image of cross-sectional transmission electron microscopy from the sample processed with dew-point of –20°C. Thick Mn-O oxide layer is visible in (C) and Al-Si-O oxides were found at the interface of top Mn-O oxide and ferrite as can be seen (D) and (E). (F) is the Mn distribution showing Mn-depetion right below the Al-Si-O layer. FCC, face centered cubic; TWIP, twinning-induced plasticity.

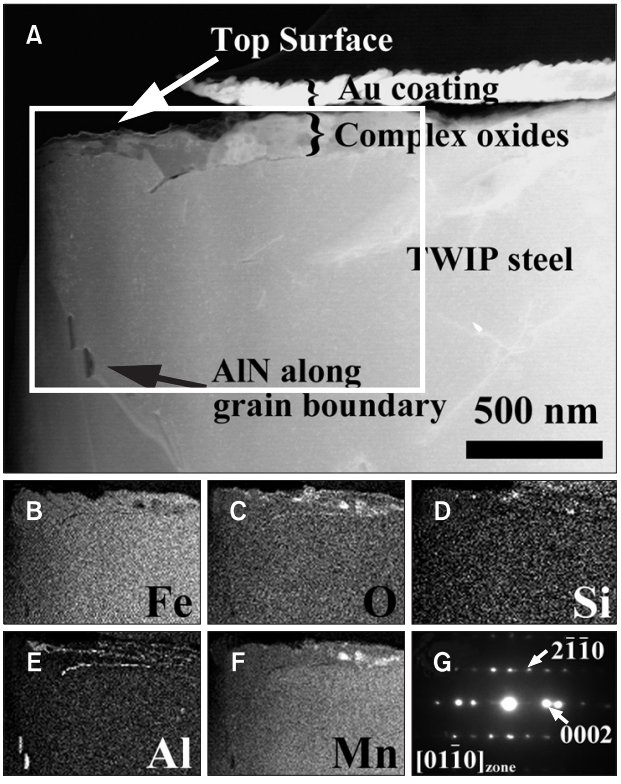

Fig. 6. Microstructure and elemental distribution of the sample processed with –40°C dew-point (DP). Distribution and number density of surface oxides dramatically reduced compared to the samples processed at DP of –20°C and above. TWIP, twinning-induced plasticity; AlN, aluminum nitride.

surface, which was identified by EDS and electron diffraction as shown in Fig. 6G. When the DP temperature was further lowered to –60°C, layered Al-O oxides broke the continuity and appeared as scattered form. Mn and Si showed strong affinity and always appeared in the mixture of Mn, Si, and O at the surface, or, just below the surface. AlN precipitates were found both inside grains and in grain boundaries in the depth range of 0.3~1 μm.

DISCUSSION

Changes in the surface Mn-O oxides can be explained by the relative amount of oxygen in the process environment. Oxygen partial pressure, which is equilibrated with water vapor pressure, is a critical parameter determining the DP temperature. Surface becomes more reducing environment when the oxygen partial pressure is reduced to provide lower DP. When surface is exposed to the higher partial pressure of oxygen, Mn and O move in opposite direction as shown in the 0°C of DP, i.e., Mn moves out of the bulk while O move into the bulk. Mn depletion and networked oxides in Fig. 2B were the results of Mn out-diffusion and the oxygen-penetration. Mn-O oxide at the surface was the result of Mn out-diffusion from the matrix, and the networked oxides at the ferrite grain boundaries were from the reaction of penetrated oxygen with the alloying elements. Once the concentration of Mn in the TWIP-aided steel matrix fell below the level to maintain austenitic phase as a result of out-diffusion, face centered cubic (FCC) phase of the matrix transformed to body centered cubic (BCC) ferrite. The solubility limits of Mn in each phase determine the phase boundary, which can be seen as sharp interfaces between ferrite and austenite in Fig. 2A. The transformed ferrite grains did not show crystallographic relationship between ferrite grains and austenite matrix.

Difference in the elemental distribution in the networked oxides could be explained by the relative diffusion rates. The networked oxides showed high concentration of Al and Si in the oxide core, and then the Mn distribution surrounding the core Al-Si-O oxides. Aluminum and Silicon distribution in Fig. 2F shows sharp distinct signals, while Mn and O distributions are broader as can be seen in the rectangles in Fig. 2D-F. Diffusivities of Mn, Si, O, and Al were reported as 9.06×10^{-4}, 1.46×10^{-3}, 8.01, and 5.56×10^{-4} $\mu m^2\ s^{-1}$ (Oikawa, 1983; Tong et al., 2003; Huin et al., 2005), respectively. Oxygen, moved into the bulk from the surface, readily formed oxides with Al and Si because of its high diffusivity. Mn-O oxides, on the other hand, formed at outside of pre-existing Al-Si-O oxides because of relatively low diffusivity. The similar layered oxide formation, controlled by the diffusivity kinetics, was reported earlier in other ally steel systems (Oikawa, 1983; Huin et al., 2005).

Calculations of THERMOCALC revealed that MnO/Mn_3O_4 were the stable oxides –20°C and above, and Al_2MnO_4/Mn_2SiO_4 for –40°C DP and below. Experimental XTEM observation of oxides showed in good agreement with THERMOCALC results for the low-DP processed sample, but not well in the samples processed at high DP because it showed the shell structure of Al-Si-O and Mn-O. Discrepancy of oxides between the THERMOCALC and experimental results at high DP was due to the relative diffusion rates of the alloying elements.

CONCLUSIONS

The distributions and the number density of surface and sub-surface oxides structure revealed dramatic change when the DP processing temperature changed from –20°C and –40°C for the TWIP-aided steel studied. The Mn-O oxides, formed on the surface with high DP, were contributed by the Mn out-diffusion sourced from the near-surface matrix, which turned FCC matrix into polycrystalline BCC ferrite. Oxygen penetrated into the matrix following the fast diffusion path, along the grainboundaries of ferrite. DP temperature should be maintained at –40°C or below to minimize the formation of continuous Mn-O oxides on the surface.

REFERENCES

Gavriljuk V G, Tyshchenko A I, Razumov O N, Petrov Y N, Shanina B D, and Berns H (2006) Corrosion-resistant analogue of Hadfield steel. *Mat. Sci. Eng. A* **420**, 47-54.

Grässel O, Krüger L, Frommeyer G, and Meyer L W (2000) High strength Fe-Mn-(Al, Si) TRIP/TWIP steels development–properties–application. *Int. J. Plasticity* **16**, 1391-1409.

Hadfield H A (1956) *Manganese Steel* (Olver and Bald, London).

Huin D, Flauder P, and Leblond J B (2005) Numerical simulation of internal oxidation of steels during annealing treatments. *Oxid. Met.* **64**, 131-167.

Li X S, Baek S I, Oh C S, Kim S J, and Kim Y W (2008) Dew-point controlled oxidation of Fe-C-Mn-Al-Si-Cu transformation-induced plasticity-aided steels. *Scripta Mater.* **59**, 290-293.

Mintz B, p. 551, Galvatech 2001: proceedings of the 5th International Conference on Zinc and Zinc Alloy Coated Steel Sheet, June 26-28, 2001, Brussels, Belgium /editor: Marcel Lamberights.

Oikawa H (1983) Lattice diffusion of substitutional elements in iron and iron-base solid solutions. *Technol. Rep. Tohoku. Univ.* **48**, 7-77.

Sato A, Soma K, Chishima E, and Mori T (1982) Shape memory effect in γ⇄ε transformation in Fe–30Mn–1Si alloy. *Acta Matall.* **30**, 1177-

1183.

Tomota Y, Strum M, and Morris J W (1987) The relationship between toughness and microstructure in Fe-high Mn binary alloys. *Metall. Trans. A* **18**, 1073-1081.

Tong W P, Tao N R, Wang Z B, Lu J, and Lu K (2003) Nitriding iron at lower temperatures. *Science* **299**, 686-688.